Journal of Power Sources 196 (2011) 7136–7143

Contents lists available at ScienceDirect

Journal of Power Sources

journal homepage: www.elsevier.com/locate/jpowsour

Area specific resistance of oxide scales grown on ferritic alloys for solid oxide fuel cell interconnects

Stefan Megel*, Egle Girdauskaite, Viktar Sauchuk, Mihails Kusnezoff, Alexander Michaelis

Fraunhofer Institute for Ceramic Technologies and Systems, Winterbergstraße 28, 01277 Dresden, Germany

ARTICLE INFO

Article history:
Received 17 June 2010
Received in revised form 16 August 2010
Accepted 2 September 2010
Available online 15 September 2010

Keywords:
SOFC
Oxide layer
ASR
Interconnect
Contact
Protection layer

ABSTRACT

Planar solid oxide fuel cells (SOFC) are considered to be power generators with high efficiency and low emission at small power units (1–200 kW_{el}). Many prototype systems are already successfully realized. For mass production the costs have to be reduced and the long-term stability has to be enhanced. Power losses <0.5%/1000 h is the target value for stacks in stationary SOFC-based power systems. To reach this goal, the factors influencing degradation have to be found and reduced. In this work the interaction between interconnect and different ceramic materials such as perovskites ($La_{0.8}Sr_{0.2}(Mn,Co)O_3$, $La_{0.65}Sr_{0.3}MnO_3$, $La_{0.65}Sr_{0.3}(Mn,Co)O_3$) and spinels ($(Mn(Co,Fe)O_4$, $(Cu,Ni)Mn_2O_4$) was investigated on the cathode (air) side of conventional ferritic interconnect materials (CroFer22APU, ITMLC, ZMG232L). The method to determine the value of the area specific resistance between interconnect and contact layer ($R_{\#ICC}$) within a tolerance of 10% has been developed to provide reliable data for ASR values and their degradation.

The $R_{\#ICC}$-value increases with annealing time. The degree of this increase depends on used materials and their combination. The spinel contact layers form a thin dense ceramic layer at the beginning of the annealing process. This layer reduces the oxidation rate of the alloy. Because of this protection layer a thinner oxide scale grows and the ASR aging rate is much lower (0.4–0.9 $m\Omega\,cm^2$/1000 h). The comparison of the aging rates of different alloys with $La_{0.8}Sr_{0.2}(Mn,Co)O_3$ contact layer reveals remarkable differences: 3.1 $m\Omega\,cm^2$/1000 h for CroFer22APU, 10.9 $m\Omega\,cm^2$/1000 h for ITMLC and 21.2 $m\Omega\,cm^2$/1000 h for ZMG232L.

The degradation in a stack has been determined from the $R_{\#ICC}$-values and geometric factors. The impact of oxidation at the cathode side of interconnect is about one third of the total stack degradation. The method opens the possibility for comparing area specific resistances of special material combinations with high accuracy. By optimized material combinations the degradation in stacks can be reduced to <0.5%/1000 h.

1. Introduction

Planar, bipolar SOFC needs interconnects for separating gas and air flow, electrical contacting and mechanical stabilization of the cells in stack. In the past years several types of ferritic stainless steels have been examined as potential candidates for stack interconnects, because of their low resistivity of oxide scale, easy processing and low-cost manufacturing. The thermal expansion coefficient (TEC) of the ferritic alloy Crofer22APU [1,2] is well suited to the TEC of the electrolyte and the material has a sufficient stability at temperatures about 800 °C.

At high temperatures oxide layers grow on the surface of ferritic stainless steels. The oxide scale with relatively good electrical conductivity protects alloy from chromium evaporation and breakaway oxidation. Ceramic protection layers affect the oxide formation at the interconnect and are important for the long-term operation of a stack. The oxide layers grow under typical SOFC operating conditions with rising time, cause an increase of the area specific resistance (ASR) and are partially responsible for stack degradation. Many efforts were made to diminish disadvantages of using ferritic alloys for SOFC interconnect materials. The common strategy to minimize the oxide scale growth is the realization of a gas-tight, highly electrical conductive protection layer with a thermal expansion coefficient (TEC) matched to the interconnect. Different coatings were tested in order to ascertain the most suitable SOFC interconnect protection and contact material.

Perovskites (ABO_3) with lanthanum and strontium on the A-site and manganese on the B-site as well as different manganese, cobalt, or copper-based spinel materials offer relatively good

* Corresponding author. Tel.: +49 351 2553 505; fax: +49 351 2554 187.
E-mail address: Stefan.Megel@ikts.fraunhofer.de (S. Megel).

0378-7753/$ – see front matter © 2010 Elsevier B.V. All rights reserved.
doi:10.1016/j.jpowsour.2010.09.003

Table 1
Selected ferritic alloys for investigations.

Name	Charge	Manufacturer	Date of delivery
Crofer22APU	170845	Thyssen Krupp VDM	06/2006
ITMLC	007	Plansee SE	08/2006
ZMG232L	LM647	Hitachi Metals LTd.	12/2006

chemical stability, high electrical conductivity and a TEC near to the interconnect and electrolyte one.

There are different approaches for measuring the ASR values of the oxide scale formed between ferritic alloy and ceramics. However, the measured ASR values are actually a sum of different resistances consisting of interconnect-, contact layer- and oxide scale resistances. The separation of those different parts of resistances is complicated. A great scattering of absolute ASR values and their change with the time appears due to various assemblies of samples and different material compositions [3]. For example, the ASR values of the oxide scale for similar material combinations ($La_{0.8}Sr_{0.2}(Mn,Co)O_3$ and CroFer22APU) range from 0.8 to 12 $m\Omega\,cm^2$ [4–7]. The rate of the ASR value increment of the oxide scale is very important for the estimation of the degradation of a stack. This rate varies from 0.5 to 25 $m\Omega\,cm^2/1000\,h$ for above mentioned material combination and shows the importance to find appropriate samples to measure reliable ASR values and their behavior over time.

The goal of this work is to calculate a contribution of ASR of oxide scale in contact with ceramic layer to the total ASR of the stack and to degradation rate for different interconnect materials. We demonstrate an approach for the determination of ASR of the oxide scale and show the impact of appropriate material combinations of different alloys with protection or contact layer on the degradation rate of ASR due to oxide scale growth.

2. Experiments

2.1. Oxidation investigations of Crofer22APU, ITMLC and ZMG232L

We investigated the formation of the oxide scale on the surface of metallic interconnect after oxidation in air atmosphere to find a correlation between resistance increase and parameters of the oxide scale. An important reference value for the metallic interconnect materials is the weight gain of the sample. The samples of the size 15 mm × 15 mm × 0.5 mm were prepared from different ferritic alloys (Table 1) and were annealed at 850 °C for different times to evaluate the oxidation behavior parallel to the ASR measurements. Nine specimens were prepared from each ferritic alloy for different oxidation duration. Three of nine samples were coated with LSMC perovskite protective layers by roll-coating. The uncoated and coated samples were annealed in air at 850 °C. The first set of specimens was removed from the furnace after 800 h and the next ones after 1600 h and 3200 h. The weight gain of each sample was determined by a Sartorius (LA 230 s) balance before and after annealing. For comparison the values were normalized to the surface area of the sample.

2.2. Measurements of ceramic contact layer

A four-point probe method was used to measure the resistivity of the low temperature sintered contact layer materials (Fig. 1). The measurements were performed under static air conditions comparable to the measurements in [8]. Minimum two samples for each combination were measured and the average values were calculated.

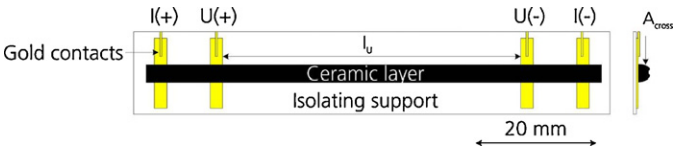

Fig. 1. Schematic diagram of the sample with ceramic rib made of paste to measure the resistivity of low temperature sintered ceramic.

The temperature in the furnace corresponds to the joining profile of the stack (920 °C/2 h → 850 °C/800 h). The measurements were carried out with thermal cycles after 800, 1600, and 3200 h of oxidation. A constant current of 0.1 A with offset compensation was applied. The resistivity ρ_{Meas} was calculated using the equation (1):

$$\rho_{Meas} = R_{Ohm} \cdot \frac{A_{cross}}{l_U} \quad (1)$$

where R_{Ohm} is the measured resistance, A_{cross} is the cross section area of the sample, and l_U is the distance between the potential contacts.

A profilometer (Fries Research Technologies GmbH) was used to determine the cross section area. For this purpose, the height profile of the ceramic rib was recorded on five different points. The cross section area was defined by integration. The uncertainty for the resistivity measurement given by such estimation of cross section area was ±4.6%.

A four-point probe resistance measurement, where corresponding current and voltage wires were directly connected to the ceramic layer, insures that contacting of ceramic ribs influences neither the absolute value nor long-term behavior of the resistance. Three different perovskites: $La_{0.8}Sr_{0.2}Mn_{0.9}Co_{0.1}O_3$, $La_{0.65}Sr_{0.3}MnO_3$, $La_{0.65}Sr_{0.3}Mn_{0.9}Co_{0.1}O_3$ and two spinels: $MnCo_{1.9}Fe_{0.1}O_4$, $Cu_{0.6}Ni_{0.4}Mn_2O_4$ were chosen from a broad field of contact or protection ceramics [3,9–13]. They give information about influence of substoichiometry, different amount of strontium and presence of cobalt on ASR of the oxide scale. The compound $Cu_{0.6}Ni_{0.4}Mn_2O_4$ was synthesized from the binary oxides Mn_2O_3, CuO and NiO at temperatures 1050–1100 °C in air using a common solid state reaction process, the other powders for preparation of contact materials were supplied by company Staxera GmbH (Dresden, Germany).

In the following text the ceramic materials are abbreviated as:

$La_{0.8}Sr_{0.2}(Mn,Co)O_3$	LSMC
$La_{0.65}Sr_{0.3}MnO_3$	uLSM
$La_{0.65}Sr_{0.3}(Mn,Co)O_3$	uLSMC
$Mn(Co,Fe)O_4$	MCF
$(Cu,Ni)Mn_2O_4$	CNM

2.3. Measurements of ASR between interconnect and ceramic contact

The sample setup was optimized in several efforts and is illustrated in Fig. 2. The asymmetric assembly of current- and voltage contacts was chosen to keep the uniform current distribution

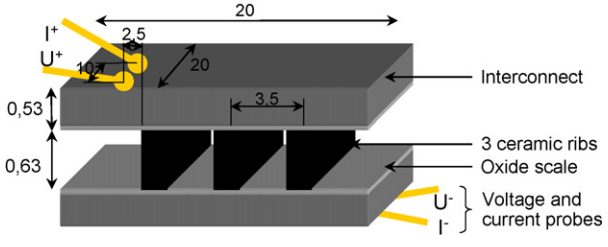

Fig. 2. Sample assembly for ASR measurements between interconnect and ceramic contact (dimensions in mm).

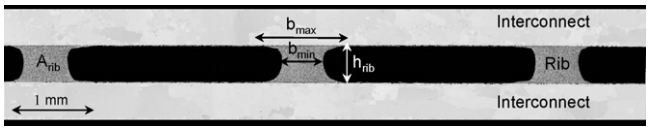

Fig. 3. Real geometry of a sample for ASR measurement between interconnect and contact layer.

through the sample. A specially developed paste (applied also in the stacks) with solid phase content up to 82% and with high viscosity (binder on basis of ethyl cellulose) was used to contact the ribs. This paste keeps its shape after application by dispensing. Three ribs made of ceramic material were dispensed on the surface of sheets (size 20 mm × 20 mm × 0.53 mm) of Crofer22APU, ITMLC and ZMG232L and then contacted with a second similar sheet to obtain a symmetric sample (Fig. 2). Spacers were inserted between two sheets to keep the height of the ribs constant. The samples were inserted into a furnace (Nabertherm GmbH M11/HR), connected with the measuring equipment and heated up to operating temperature. Each sample was loaded with 250 g in order to achieve a reliable mechanical and electrical contact between both sheets during the measurement. The measurements were carried out similar to the resistivity measurements, however a current of 0.5 A were applied.

The measured resistance reflects a performance of the complete sample as a function of annealing time. The measured resistance has to be separated into corresponding shares. The geometry of each sample has to be exactly determined by polished cross-sections of embedded samples (Fig. 3) with two component epoxy resin (Epofix Struers A/S). The width, height and cross-section area of each rib were established using the measuring microscope (Olympus STM-MJS with a measuring table MMDC 201).

For characterization of the microstructure and composition of the samples after ASR measurements, cross-sections were examined with a field emission scanning electron microscope (FESEM, Gemini 982, Leo). For a more intensive element contrast, the back scattered electrons mode at around 8 keV were used. The chemical compositions of the sample layers were established with an energy dispersive X-ray device (Oxford Inca) by point scan, line scan and surface scan analyze.

2.4. Tests of SOFC-stacks

The MK100 stack design of the Staxera GmbH was used for investigation of the cathode contacting [19]. The stack consists of a cell with a 3YSZ (3 mol Yttria stabilized Zirconia) electrolyte, of the interconnect made of Crofer22APU without protection layer and of LSMC contact ribs. A two-cell stack heated by an oven was chosen because of the low temperature gradient over the cells. The stack was sealed with a sealing glass by an especial heat up process. After the sealing process the stack operated at constant current of 309 mA cm^{-2} over time in a gas mixture of 50% N_2–40% H_2–10% H_2O and 10 Nl min^{-1} air.

3. Results and discussion

3.1. Oxidation behavior of interconnect materials

Fig. 4 represents the diagrams of the weight gain and of the oxide scale thickness of studied alloys in dependence on oxidation durability at 850 °C in air. The general trend of both diagrams is similar. ITMLC samples show the lowest weight gain according to this investigation. The samples of CroFer22APU and ZMG232L increase their weight nearly equally at the beginning of the oxidation process. The oxidation of Crofer22APU obeys almost a parabolic rule $x = kt^{1/2}$ of Wagner's theory for the whole period investigated [14,15], whereas the dependence of the process of the weight gain is more complicated in the ZMG232L alloy. After 1600 h, the weight increases more rapidly in the ZMG232L samples. Accelerated oxidation of alloy ZMG232L can be caused by the loss of Chromium from the matrix material accompanied by the breakaway oxidation [16,17] and the real oxidation process of the alloy surface can be described according to the formula $x = kt^n$. The value n can range from $0 < n < 1$ depending on the material and the stage or duration of oxidation [18]. It should be noted that the diagram of the oxide scale gain does not correctly reflect the oxidation process in materials because breakaway oxidation starts at the edges of the sample, and such areas can be unintentionally omitted during the cutting of the samples.

The samples with LSMC roll-coating protection layer have lower rates of weight gain and of the oxide scale growth. The breakaway oxidation takes place in the coated material after much longer oxidation time in comparison to uncoated samples. Although the protection layers are not dense and remain permeable for gases, an access of gaseous oxygen species to the interconnect is remarkably reduced in comparison with uncoated samples. Correspondingly, this reduces the corrosion rate of the interconnect surface. The experiments have clearly shown that even simple porous protection layer inhibits remarkably the oxidation process of the interconnect material.

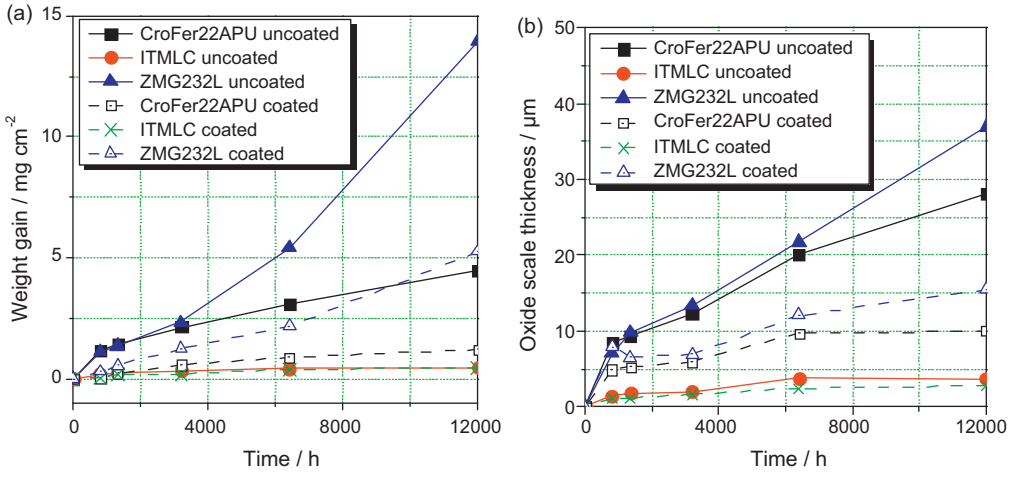

Fig. 4. Weight gain (a) and oxide scale thickness (b) of different alloys during oxidation at 850 °C in air.

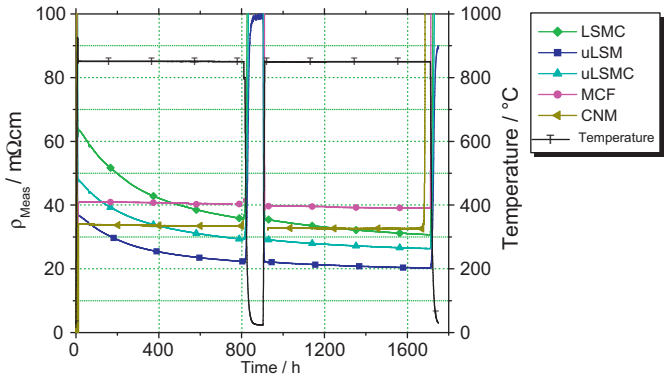

Fig. 5. Resistivity of different materials for contact layer as a function of time.

3.2. Resistivity of contact layer

Fig. 5 demonstrates resistivity of contact layers as a function of annealing time at 850 °C. The resistivity of all perovskites decreases during annealing time due to continuous sintering of powder particles. The resistivity of MCF and CNM spinels were almost constant. The contact layers made from MCF and CNM powders have better sintering activity and lower sintering temperature. Therefore they sinter faster than perovskite powders which have a similar packing density. Hence the resistivity of spinels reaches much faster a value which does not change or changes very little during annealing at 850 °C. After 1600 h annealing the MCF and CNM spinels had a resistance of about 39 and 33 mΩ cm (porosity not considered), respectively. The lowest resistivity of about 20 mΩ cm exhibited uLSM perovskite. The resistivity of the low temperature sintered ceramic is not corrected by the porosity to get values of the bulk material. The resistivity of the bulk material at 850 °C in air is in the range of 4–16 mΩ cm [3].

3.3. Measuring principle and validation

3.3.1. Results of ASR measurements

The resistivity of eight samples with the same material combination (Crofer22APU with LSMC contact layer) was measured in order to determine the reproducibility of estimation of ASR values of the oxide scale. Results are displayed in Fig. 6. All samples show a comparable values with decrease of resistance in the first 100–150 h of annealing followed by subsequent linear rise. No resistance change was observed by increasing current used for measurement up to 0.5 A. This demonstrates the ohmic behavior of the samples. The

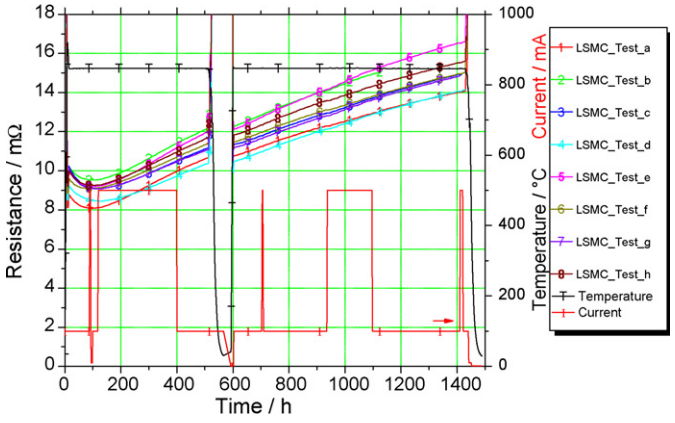

Fig. 6. Resistance of eight samples with the same material combination (Crofer22APU with LSMC contact layer) as a function of annealing time.

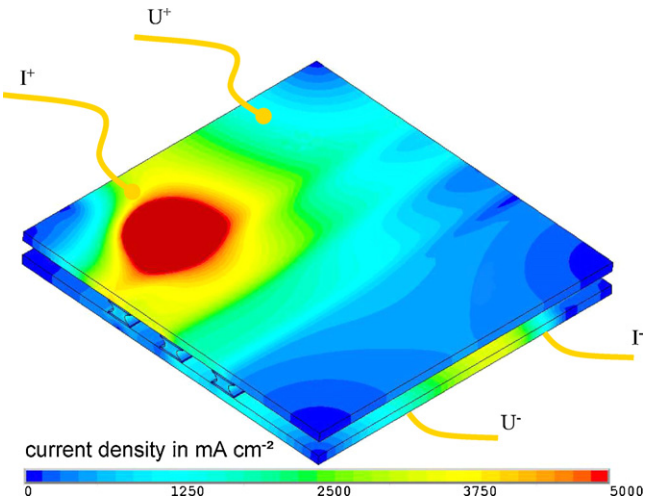

Fig. 7. Three-dimensional simulated current distribution in the sample LSMC_Test_f during 150 h oxidation with the position of contact wires.

applied current did not modify the composition of the contact layer as well as the oxide scale.

3.3.2. 3D-simulation of $R_{\#ICC}$-values

Since the measured resistance is the sum of contributions of different resistances of contact layer, oxide scale, interconnect and as well as of the influence of test equipments, it is necessary to separate these resistances. The resistivity of interconnect is known from the data sheet of Thyssen Krupp VDM [2]. The resistivity of contact layer and geometry of contact ribs has been determined separately (Section 3.2). The resistance of the oxide scale and the resistance caused by interaction with the contact layer, both defined here as $R_{\#ICC}$-value, is the only unknown value. It is necessary to simulate the samples in three dimensions because of the non-uniform current distribution through the sample, especially at low $R_{\#ICC}$-values. A finite-element structural model based on Multiphysics-Code ANSYS 5.6 was used for three-dimensional mathematical simulation of the specimens with different layers (Fig. 7). The resistance of oxide scale ($R_{\#ICC}$-value) was calculated by parameter inversion and adjustment to the measured resistance.

The results of the simulations are demonstrated by the example of Crofer22APU in combination with LSMC ceramic layer and are shown in Fig. 8. At the beginning of oxidation, the contact layer had the highest contribution to the total resistance of the sample (Fig. 8a). This contribution decreases with time due to sintering of the contact layer despite the oxide scale is steadily growing. After 700 h oxidation, the contributions of contact layer and oxide scale are nearly equal. Further the total resistance is affected basically by the oxide scale. Since the resistance of growing oxides increases strongly with decreasing temperature, the oxide scale resistance dominates at lower temperatures, and the contribution of the contact layer (ceramic rib) has a diminishing role (Fig. 8b).

The three-dimensional simulation was carried out for all samples and is shown in Fig. 9. After 150 h the $R_{\#ICC}$-values range between 1.0 and 1.3 mΩ cm^2 and increase after 1340 h up to 4.2–5.0 mΩ cm^2 (time of heating up and temperature cycling are not included). The resistance increase ($\Delta R_{\#ICC}$-value) from 150 to 1340 h was 2.8 mΩ cm^2/1000 h. The minimum and maximum values show the scattering of the estimated ASR values. The $R_{\#ICC}$-values of eight identical samples were tested and delivered values with tolerances ±10%. Therefore the method can be used to analyze the interactions between interconnects and contact layers.

The precise definition of the specimen shape for measurement of ASR of the junction “oxide scale – contact layer” coupled with

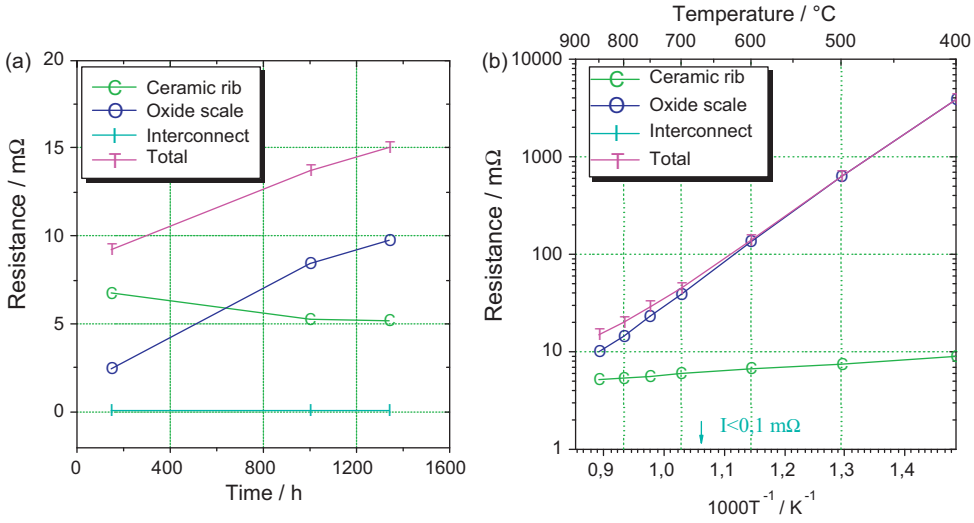

Fig. 8. Contributions of different components to the total resistance over time (a) and temperature dependence after 1340 h (b) of the sample LSMC_Test_f (in air at 850 °C) determined by simulation.

Table 2
Calculated average $R_{\#ICC}$-values for different contact layers in combination with CroFer22APU, ITMLC and ZMG232L after 150 and 3200 h at 850 °C in air.

Alloy	Contact layer									
	LSMC (mΩ cm^2)		uLSM (mΩ cm^2)		uLSMC (mΩ cm^2)		MCF (mΩ cm^2)		CNM (mΩ cm^2)	
	150[a]	3200[a]	150[a]	3200[a]	150[a]	3200[a]	150[a]	3200[a]	150[a]	3200[a]
Crofer22APU	1.0	9.1	1.0	8.6	0.9	11.0	3.2	5.4	0.7	2.0[b]
ITMLC	3.0	28.7	3.5	29.7	5.0	35.7	2.2	3.6	0.5	1.1
ZMG232L	4.2	36.0	4.1	31.7	4.9	29.2	10.3	27.8	Not measured	

[a] Annealing time (h).
[b] Value after 1600 h annealing.

simulation analysis ($R_{\#ICC}$-value) allows a new method for getting reproducible and reliable values of resistance with respect to absolute value and degradation. The deviation of ±10% of the measured value can be reduced by more accurate determination of geometry of ceramic ribs. However it exceeds the precision of measurements by conventional methods and is sufficient for obtaining information about absolute values as well as degradation behavior of different contact layers.

3.4. $R_{\#ICC}$-values of different material combinations

For determination of $R_{\#ICC}$-values the samples were oxidized for 150, 1600 and 3200 h. The determined $R_{\#ICC}$-values after 3200 h measurement are summarized in Table 2.

The growth of the oxide scale during the long-term annealing is the main reason for increasing resistance in the specimens. Application of spinel layers for Crofer22APU and ITMLC shows considerable decrease of $R_{\#ICC}$-values in comparison with the samples containing perovskite layers. Iron diffused from the matrix alloy material was found in $(Mn,Cr)_3O_4$ oxide scale of all samples investigated. The doping with Iron causes the reduction of resistivity of oxides [3].

The changes of $R_{\#ICC}$-values for different material combinations are presented in Fig. 10. These results show that contact layers on basis of MCF and CNM spinel material improve significantly the degradation behavior of Crofer22APU and ITMLC samples whereas no considerable resistance decrease was observed in samples with ZMG232L alloy. The combinations of ITMLC alloy with spinel (MCF and CNM) contact layers exhibited almost tenfold lower $R_{\#ICC}$-

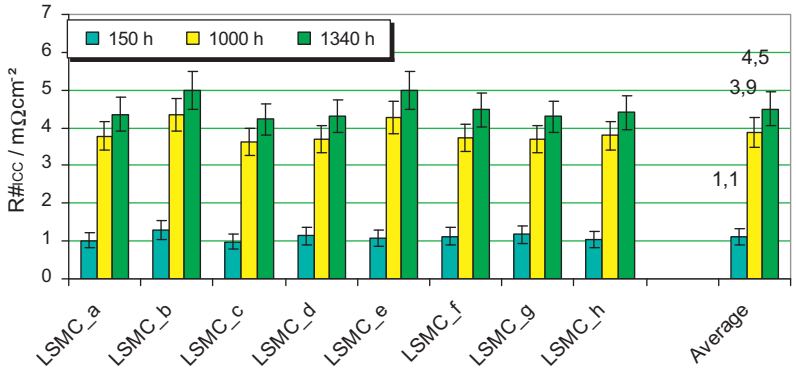

Fig. 9. Calculated $R_{\#ICC}$-values after 150 h, 1000 h, and 1340 h oxidation at 850 °C in air.

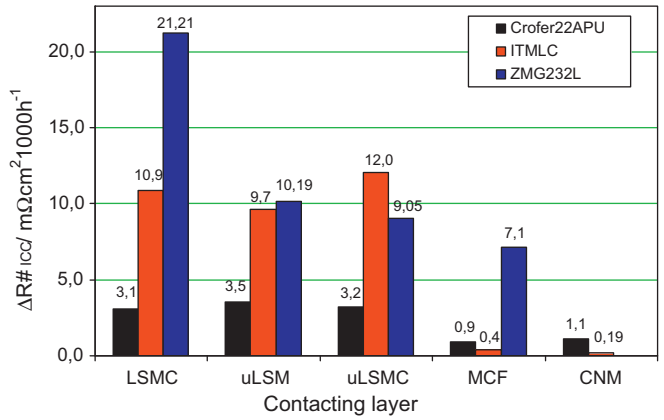

Fig. 10. Calculated degradation rates of the contact resistance interconnect – contact layer for CroFer22APU, ITMLC and ZMG232L in combination with different contact materials.

values than specimens with perovskite contact layer and showed the lowest degradation rates (MCF: $\Delta R_{\#ICC} = 0.4\,m\Omega\,cm^2/1000\,h$ and CNM: $\Delta R_{\#ICC} = 0.19\,m\Omega\,cm^2/1000\,h$). Different $R_{\#ICC}$-values and degradation rates of various combinations can be explained by formation of different oxide scales between interconnect and contact layer as well as by different thickness of the oxide scale (Figs. 11 and 12). As observed in Fig. 11a–c all three perovskite contact layers (LSMC, uLSM and uLSMC) formed on Crofer22APU a very similar double oxide scale consisting of Cr_2O_3 and $(Mn,Cr)_3O_4$. This result shows that the different contents of Sr and Co in the perovskite materials have an unimportant influence on the $R_{\#ICC}$-value. In contrary to CroFer22APU and ZMG232L alloys, ITMLC with perovskite coating forms only one very porous Chromia scale. The oxide scale of ZMG232L with perovskite contact layer has a comparable double layer structure but is much thicker than on CroFer22APU (Fig. 12). The analysis of cross section of the spinel coated samples shows a very thin Cr_2O_3 layer between the contact layer and CroFer22APU or ITMLC alloy after ASR measurements. A densified zone of the contact layer was found close to the Cr_2O_3 layer in the samples with MCF and CNM contact layers. This densified area is referred to be a reaction zone at the interface between the interconnect and the contact layer and consist of spinel based solid solution, which has higher conductivity than other oxides growing between interconnect and contact layer. Especially, interdiffusion of iron or cobalt into the oxide scale changes the layer composition and morphology and therefore can decrease or increase the resistance of the sample. The chromium content decreases in a small

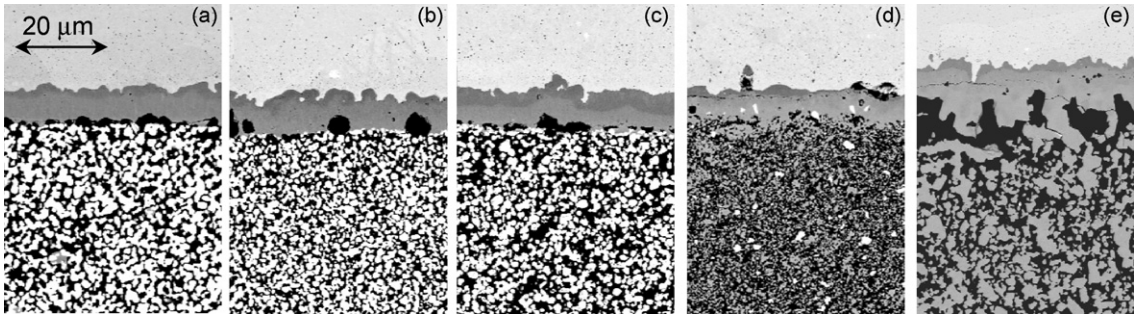

Fig. 11. Cross sections of the Crofer22APU samples in combination with LSMC (a), uLSM (b), uLSMC (c), MCF (d) and CNM (e) contact layers after 3200 h measurement at 850 °C in air.

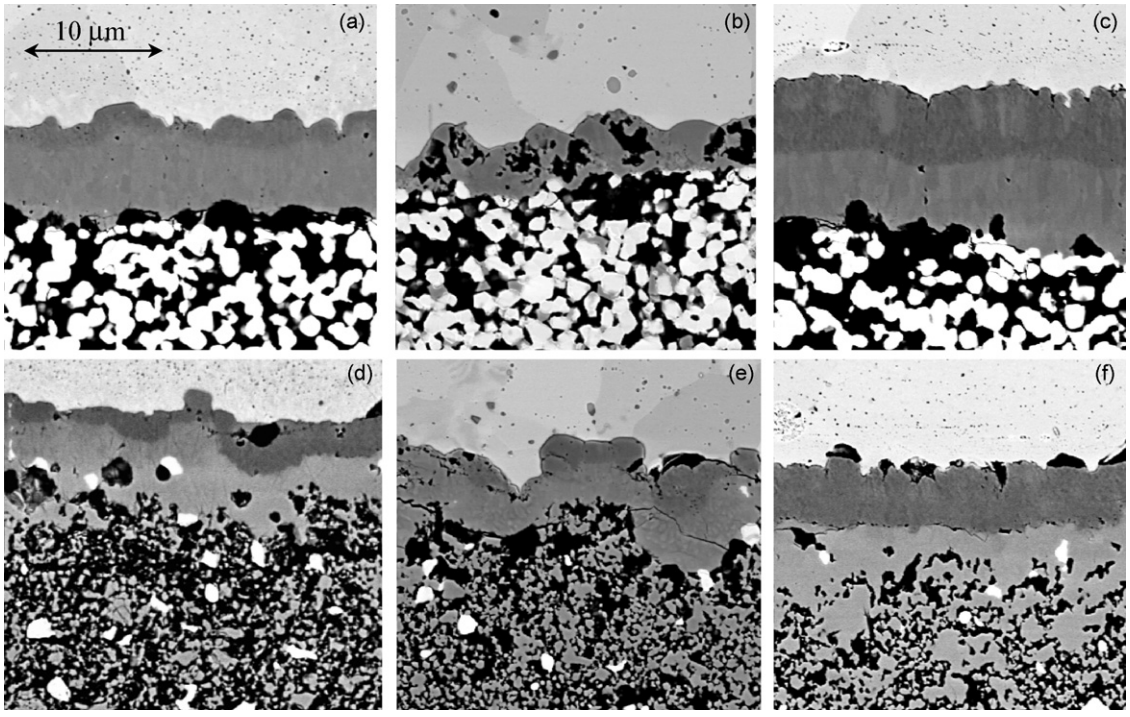

Fig. 12. Cross sections of different alloys with LSMC and MCF contact layers after 3200 h oxidation at 850 °C in air: (a) CroFer22APU + LSMC; (b) ITMLC + LSMC; (c) ZMG232L + LSMC; (d) CroFer22APU + MCF; (e) ITMLC + MCF; (f) ZMG232L + MCF.

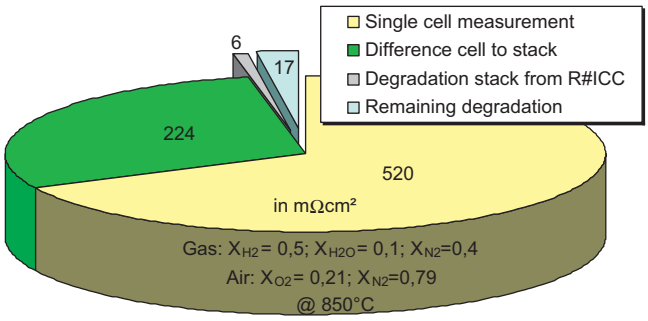

Fig. 13. Losses in the stack and degradation rates as example of a stack with LSMC ceramic ribs and CroFer22APU interconnect.

interface zone between chromia layer and contact layer. It is important for the use in SOFC-stacks, that the material of the densified zone has no chromium content. This densified zone protects the interconnect against further oxidation and chromium evaporation.

Figs. 11 and 12 show that all coatings have good adherence to the interconnects. ZMG232L forms the thickest oxide scale with all contact layers, what is reflected in the highest $R_{\#ICC}$-values and degradation rates in comparison with other ferritic alloys analyzed. The Cr_2O_3 scale between ITMLC and perovskite contact layers is very thin and porous. Nevertheless, the resistance of the samples is very high. In these samples a high porosity of the oxide scale formed between interconnect and contact layer has more influence on degradation than thickness of growing oxide scale.

A porosity correction of the $R_{\#ICC}$-values makes no sense. The porosity analysis by images has a high uncertainty and does not reflect the real contacted area.

3.5. Determination of resistance contribution to the stack performance and degradation

The corrected ASR of one arbitrary chosen cell in a stack with the material combination of Crofer22APU and LSMC increased from $R_{\#Stack} = 744\,m\Omega\,cm^2$ to $767\,m\Omega\,cm^2$ within the first 1000 h operating time (Fig. 13). The measurements of the single cell showed a constant resistance of $520\,m\Omega\,cm^2$. The discrepancies between the single cell and stack data, coming from measurement differences, arise from inhomogeneous temperature and gas distributions on the anode side of the single cell, different activation of the anode as well as from the contacting of the cathode. In the stack the same contact layer like in samples for $R_{\#ICC}$-validation was used to get a comparable porosity, reactions and oxide scale.

There is no significant oxide scale in the beginning of stack operation. Therefore the contribution of the oxide scale to the total resistance of the stack could be neglected in the first hours of stack operation. By normalizing the $\Delta R_{\#ICC}$-value of $3.1\,m\Omega\,cm^2/1000\,h$ of the material combination LSMC with CroFer22APU to geometrical parameters of the stack, a degradation rate of $\Delta R_{\#ICC,Stack} = 6.2\,m\Omega\,cm^2/1000\,h$ can be calculated. The oxide scale formation between interconnect and contact layer has a significant contribution to the total degradation of the stack $\Delta R_{\#ICC,Stack}/\Delta R_{\#Stack} = 27\%$ of the measured stack degradation of $\Delta R_{\#Stack} = 23\,m\Omega\,cm^2/1000\,h$. The decrease of the oxide scale growth would reduce this value. An application of MCF as protection layer would lead to the lower degradation rate of the ASR ($\Delta R_{\#ICC,Stack} = 1.9\,m\Omega\,cm^2/1000\,h$) and therewith would enhance the long-term stability of the stack. Reduction of degradation by using spinel coatings was confirmed for several stacks [19]. The 10-cell stack (MK200 Design of Staxera GmbH) with different coated interconnects was tested at IKTS. The cells, which were contacted with uncoated plates and LSMC contacting layers showed a degradation rate of 3–4.3%/1000 h, whereas the cells with spinel (MCF and CNM) coated interconnects had degradation rates of 0.23–0.27 and 0.17%/1000 h, respectively [20].

Formation of the oxide scale on the surface of interconnect is one of possible reasons influencing the stack degradation. By minimizing the impact of this process the other factors such as chromium poisoning of the cathode, anode agglomeration, formation of oxide scale on the anode side of the interconnect become more important for the total stack degradation.

4. Conclusions

The long-term stability of the stacks can be effectively enhanced by special protection layers. The newly developed design of specimens, with subsequent procedure of analysis for the determination of interactions between interconnect and contact layer provided reproducible ASR values and allowed the optimization of protective coatings in terms of initial ASR value and degradation rate. This testing method can provide reliable values of ASR between interconnect and contact layer. For the Crofer22APU samples contacted with LSMC ribs, the ASR value of the oxide scale was $R_{\#ICC} = 1.0\,m\Omega\,cm^2$ after 150 h oxidation at 850 °C and increased after 3200 h up to $R_{\#ICC} = 9.1\,m\Omega\,cm^2$. The degradation rate $\Delta R_{\#ICC} = 3.1\,m\Omega\,cm^2/1000\,h$ was established as characteristic value for the interface between LSMC and Crofer22APU. The ASR contribution of oxide scale ($R_{\#ICC} = 1.0\,m\Omega\,cm^2$) to the initial total resistance of the stack was less than 1% after 150 h. However their impact on total degradation rate was very high (23–27% of total stack degradation rate). The lowest degradation rates in here analysed Crofer22APU samples with different contact layers were established for spinels MCF and CNM ($\Delta R_{\#ICC} = 0.9$ and $1.1\,m\Omega\,cm^2/1000\,h$, respectively). All used interconnect materials showed higher $\Delta R_{\#ICC}$-values with perovskite layers. Although the ASR increase of ZMG232L can be reduced by the use of MCF contact layer its value was much higher than for other material combinations. The increased weight gain after more than 1600 h oxidation and appeared breakaway oxidation makes impossible the application of uncoated ZMG322L alloy for long-term stable stack operation at 850 °C. Both Crofer22APU and ITMLC are suitable materials for application as SOFC interconnects for operation at 850 °C for more than 20,000 h, if MCF or CNM spinels are used as protective coatings. MCF and CNM layers form a dense protective layer near to the interconnect surface at the beginning of the stack operation. This layer protects the metallic interconnect from further oxidation and possibly reduces the chromium release.

Acknowledgements

The State Ministry for Economy and Technology (BMWi) and Staxera GmbH are greatly acknowledged for funding the research activities and cooperation, Plansee SE and Hitachi Metals Ltd. are acknowledged for providing the samples of the interconnect materials.

References

[1] W.J. Quadakkers, T. Malkow, J.P. Abellan, U. Flesch, V. Shemet, L. Singheiser, 4th European Fuel Cell Forum, Lucerne Switzerland, 2000, pp. 827–836.
[2] ThyssenKrupp VDM GmbH, Crofer22APU data sheet No. 4146, November 2006.
[3] S. Megel, Kathodische Kontaktierung in planaren Hochtemperaturbrennstoffzellen, Ph.D. Thesis, ISBN 978-3-8396-0066-5, Band 6 Schriftenreihe Kompetenzen in Keramik, Fraunhofer Verlag, Stuttgart, Germany, 2009.
[4] N. Dekker, B. Rietveld, J. Laatsch, F. Tietz, 6th European Fuel Cell Forum, Lucerne Switzerland, 2004, pp. 319–328.
[5] Z. Yang, G. Xia, P. Singh, J.W. Stevenson, Electrical contacts between cathodes and metallic interconnects in solid oxide fuel cells, Journal of Power Sources 155 (2006) 246–252.
[6] I. Mikkelsen A. R. Dinesen, P. V. Hendriksen, Interface resistance between FeCr alloys and LSM, International Symposium Solid Oxide Fuel Cells 9, 2005, Quebec, Canada, pp. 1832–1841.

[7] E. Konycheva, J. Laatsch, E. Wessel, F. Tietz, N. Christiansen, L. Singheiser, K. Hilpert, Influence of different perovskite interlayers on the electrical conductivity between $La_{0.65}Sr_{0.3}MnO_3$ and Fe/Cr-based steels, Journal of Solid State Ionics 177 (2006) 923–930.
[8] S. Megel, K. Eichler, N. Trofimenko, S. Hoehn, Electrical resistivity of low temperature sintered perovskites, Solid State Ionics 177 (2006) 2099–2102.
[9] W. Baukal, W. Kuhn, Das Elektrodenverbindungsmaterial ein zentrales Bauelement in Hochtemperatur-Brennstoffzellen Teil I Überblick, Journal of Power Sources 1 (1976) 91–97.
[10] M. Kertesz, I. Riess, D.S. Tannhauser, Structure and Electrical Conductivity of $La_{0.84}Sr_{0.16}Mn0_3$, Journal of Solid State Chemistry 42 (1982) 125–129.
[11] Z. T. Zhang, L. Ouyang, Z. L. Tang, Synthesis and characteristics of $La_{1-x}Sr_xMnO_3$ for cathode materials of SOFC, International Symposium Solid Oxide Fuel Cells 4, 1995, Yokohama, Japan, pp. 502–511.
[12] S.C. Paulson, H. Ling, R.N. Basu, A. Petric, V.I. Birss, 26th Risø International Symposium on Materials Science, Roskilde, Denmark, 2005, pp. 305–310.
[13] V. Sauchuk, M. Kusnezoff, N. Trofimenko, S. Megel, H.-P. Baldus, A. Reinert, 8th European Fuel Cell Forum, Lucerne, Switzerland, 2008, p. A902.
[14] C. Wagner, Beitrag zur Theorie des Anlaufvorgangs, Zeitschrift für physikalische Chemie (1933) 25–41.
[15] G.C. Wood, D.P. Whittle, The mechanism of breakthrough of protective chromium oxide on FeCr alloys, Journal of Corrosion Science 7 (1967) 763–782.
[16] B. Craig, Fundamental Aspects of Corrosion Films in Corrosion Science, ISBN 0-306-43623-X, Plenum Press, New York, USA, 1991.
[17] P. Huczkowski, N. Cristiansen, V. Shemet, L. Singheiser, W.J. Quadakkers, 6th European Fuel Cell Forum, Lucerne, Switzerland, 2004, pp. 1594–1601.
[18] G. Wood, High temperature oxidation of alloys, Journal of Oxidation of Metals 2–1 (1970) 11–57.
[19] C. Wunderlich, Fuel Cell Seminar 2007, San Antonio, USA, 2007.
[20] Q. Fang, M. Heinrich, C. Wunderlich, CroFer22APU as a SOFC interconnect material, 9th European Fuel Cell Forum, Lucerne, Switzerland, 2010, B403.